An Unmanned Aerial Carrier and Anchoring Mechanism for Transporting Companion UAVs

Yiyong Gou[a], Lucas Dahl[b], Jan Krüger[c], Cavid Karca[d], Dean Boonen[e] and Rico Möckel[f]
DKE SwarmLab, Department of Data Science and Knowledge Engineering,
Maastricht University, Maastricht, The Netherlands

Keywords: Unmanned Aerial Carrier, Anchor Design, Companion UAV, Aerial Anchoring Mechanism.

Abstract: This paper demonstrates an unmanned aerial carrier as well as a new anchoring mechanism for connecting and transporting companion unmanned aerial vehicles (UAVs). Establishing this platform presents unique challenges including the requirements of precise localization of the platform, real-time environment mapping system, robust flight control approach, docking safety mechanism, and reliable anchor system for the companion UAV. To obtain the positioning information, a tightly-coupled visual-inertial optimization based odometry is implemented with a fisheye camera and an inertial measurement unit. A 3D map is updated in real-time using an Octomap framework. A nonlinear position model predictive controller cascaded with a DJI attitude controller is implemented for the flight control. Innovatively, we designed a lightweight anchoring mechanism for safe landing and reliable transportation of the companion UAV. Real-world experiments results suggest that the transportation system is a viable approach to transport the companion UAV, and that the proposed anchoring mechanism allows for reliable operation.

1 INTRODUCTION

Recent years have witnessed the development and exploration of a variety of multi-robot systems. In these distributed systems, robots cooperate to achieve tasks that an individual robot would not be capable of. Often the strengths of robots with different configurations and abilities are combined. Demonstrated examples of multi-robot systems include multi-drone parcel delivery (Peng et al., 2019), self-reconfigurable perception-driven modular robots (Daudelin et al., 2018), and the combination of unmanned aerial vehicles (UAVs) and unmanned ground vehicles (Yu et al., 2018; Ullah et al., 2021).

This work contributes the design and exploration of a new light-weight anchoring mechanism for aerial carrier UAVs. In addition, an aerial carrier is presented that, with the help of the proposed anchoring mechanism, can carry a small companion UAV. The combination of both UAVs is advantageous for human operators that e.g., desire to perform aerial inspections: The aerial carrier provides to the companion UAV long-distance travel, communication, and control as well as the necessary computational resources for automatic image processing. In return, the companion UAV allows reaching small areas that the carrier cannot get into. The more expensive companion UAV can also be chosen to undergo inspection operations that might lead to a loss of the UAV and thus are too risky to be handled by the higher-costs carrier UAV.

1.1 Related Work

In general, aerial robotic transportation platforms require a reliable onboard flight system which typically consists of precise localization, environment perception and flight control modules (Lutz et al., 2020). Aerial robotic localization has been investigated using computer vision (Qin et al., 2018; Bloesch et al., 2017), global navigation satellite system (Loianno et al., 2018), inertial measurements (Afrisal et al., 2019), laser (Zhang and Singh, 2014), and Ultra Wide Band (Perez-Grau et al., 2017) based methods, among which the multi-sensors fusion approach

[a] https://orcid.org/0000-0001-7544-4675
[b] https://orcid.org/0000-0002-6536-2243
[c] https://orcid.org/0000-0002-7589-7604
[d] https://orcid.org/0000-0002-8270-7418
[e] https://orcid.org/0000-0001-8096-1829
[f] https://orcid.org/0000-0001-5497-3754

Gou, Y., Dahl, L., Krüger, J., Karca, C., Boonen, D. and Möckel, R.
An Unmanned Aerial Carrier and Anchoring Mechanism for Transporting Companion UAVs.
DOI: 10.5220/0010655500003061
In *Proceedings of the 2nd International Conference on Robotics, Computer Vision and Intelligent Systems (ROBOVIS 2021)*, pages 103-112
ISBN: 978-989-758-537-1

is often utilized to obtain higher localization precision. Mostly lightweight lidar and stereo cameras are selected to provide 3D information for environment perception (Hornung et al., 2013; Lin et al., 2019). Cascade control techniques with two level controllers are generally implemented in flight control application and onboard position controller such as proportional-integral-derivative control, gain-scheduled proportional-integral-derivative control(Wasim et al., 2019), model predictive control (MPC) (Kamel et al., 2017; Kamel et al., 2016; Tzoumanikas et al., 2019), and geometric control (Lee et al., 2010) are adopted and normally followed by an off-the-shelf autopilot as the inner loop attitude controller.

With respect to the UAV docking platform, an aerial recharging docking platform was developed and implemented in (Jain and Mueller, 2020; Jain et al., 2020) and they are both tested to achieve accurate docking with the localization information provided by an indoor position tracking system. Assisted with artificial vision, a ground landing mechanism with four bowl-shape inner cones surfaces was developed for the UAV docking and recharging (Cocchioni et al., 2014), but it was designed for ground static landing and cannot ensure safety in case of the carrier wobbling that might cause the companion UAV dropping. Moreover, a UAV docking platform with the ground mobile manipulator attached with an eye-in-hand visual sensor was built and implemented with UAV (Narváez et al., 2017; Narváez et al., 2020). A special in-flight docking platform with a customized vertical mast as a docking mechanism mounted above on the aerial carrier was simulated with a quadcopter assisted by the Global Positioning System (GPS) and a computer vision process (Rocha and Robinson, 2020). In current research, the docking platforms are mostly operating on the ground or lack of the ability of environment perception, or rely on an external positioning system. Additionally, these platform are not equipped with robust fault-tolerance mechanisms which ensure reliable and safe docking.

1.2 Contributions

The contributions of this paper include the following:

1. A novel design and validation of a lightweight anchor system which is customized for docking and transporting companion UAVs.
2. Development and design of hardware and software of a custom-made aerial carrier with mounted anchoring mechanism.

2 PLATFORM HARDWARE DESIGN

Given the requirement of achieving aerial transport and anchoring for the companion UAV, the considerations concerning the platform hardware design include the structural stability, available payload, structural protection, and fault-tolerance of the anchoring mechanism and aerial carrier. In this section, we present the system hardware as shown in Figure 1.

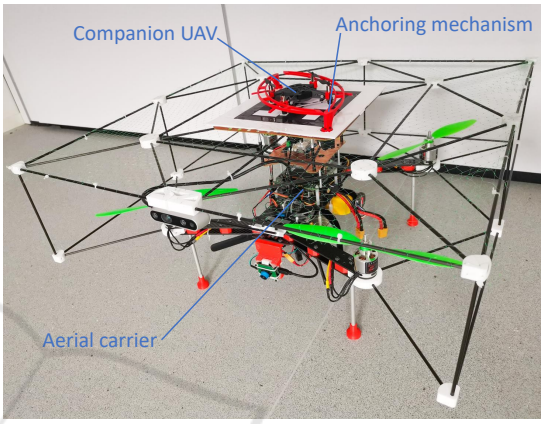

Figure 1: Aerial carrier with anchoring mechanism and attached companion UAV.

2.1 Hardware Overview

The whole system hardware consists of four major elements: (1) an aerial carrier with onboard computational resources running software for perception and control, (2) an anchor mechanism integrated onto the aerial carrier for anchoring a companion UAV, (3) a modified DJI Tello companion UAV with a changed downward camera, and (4) a ground station for monitoring and communication with the aerial platforms. Figure 2 shows a block diagram of the electronics hardware components of the carrier UAV and ground station. Table 1 provides additional specifications. With a total system weight (including aerial carrier 3.918kg, companion UAV 0.086kg, and anchoring mechanism 0.146kg) of 4.15kg, the carrier UAV reaches a flight time of up to eight minutes in operation mode.

2.2 Design of Anchoring Mechanism and Protection

The anchoring mechanism shown in Figure 3 is composed of a 3mm-thick foam board featuring a fractal marker (Romero-Ramirez et al., 2018; Romero-Ramire et al., 2019; Garrido-Jurado et al., 2016) for

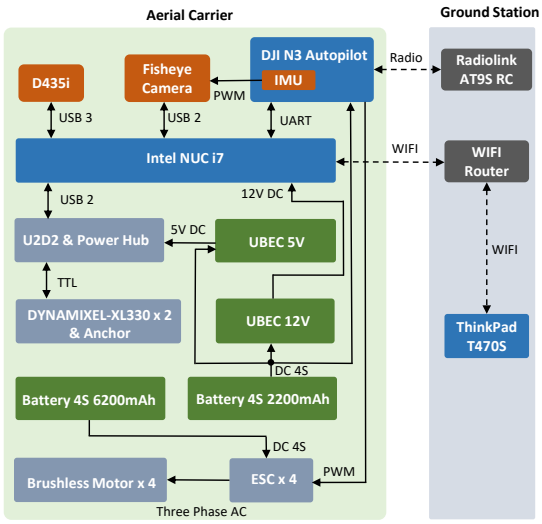

Figure 2: Ground station and electronic hardware components of aerial carrier.

Table 1: System components and specifications.

Components	Specifications
DC motor * 4	Turnigy 3542-800kv
Propeller * 4	4.7inch×11inch
ESC * 4	Skywalker 50A
Autopilot	DJI N3 (IMU)
Sensing	• AR0134 fisheye camera • Intel RealSense D435i
Servo	• Dynamixel XL-330-M228 • Dynamixel U2D2 interface
RC controller	RadioLink AT9S
Onboard PC	Intel NUC7i7DNBE 16G
Battery	• LiPo 4S 2200mAh • LiPo 4S 6200mAh
Body frame	Carbon fiber 40cm×40cm
Protection	• Carbon fiber cage 70cm×70cm • UV polyethylene nets
Anchor	• 3mm foam board 25cm×25cm • PLA 3D printed arm * 2

automatic detection by and landing of a companion UAV. After landing on the foam board (not discussed in this paper) and during aerial transport, the companion UAV is grabbed and fixated by two custom-made arms (shown in red in Figure 3) that are being controlled by two lightweight Dynamixel motors. The custom-made arms are designed to be lightweight, fault-tolerant and stiff enough to secure the companion UAV. The total weight of the anchoring mechanism (including foam board, electronics, motors, and arms) is around 172g. Each arm weighs 15g, and they are being held on by three nylon screws, respectively. The inner surface of the arm is sloped to prevent any mating surface from binding and blocking the mechanism.

In addition to the anchoring mechanism, a supportive protection structure composed of carbon fiber rods and UV stabilized polyethylene nets has been designed and attached to the aerial carrier to make the landing and anchoring process more fault-tolerant and to prevent any falling object from destroying the aerial carrier system while providing additional safety margins for the landing of the companion UAV. The total weight of this protection structure (Figure 1) is around 413g.

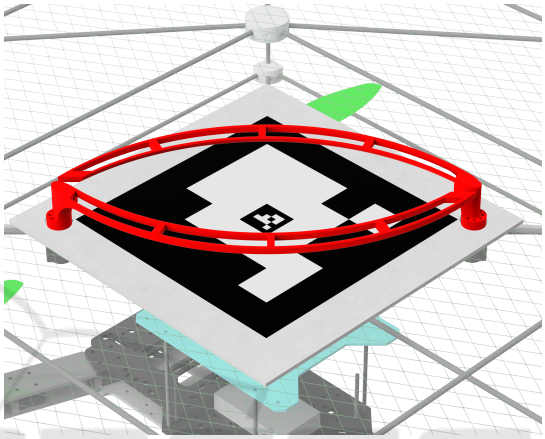

Figure 3: CAD view of the anchoring mechanism installed above the aerial carrier.

2.3 Sensors and Computation Resources

To achieve the requirements of the aerial robotic environment perception and localization, we choose a 1/3 inch 1.2MP global shutter monochrome camera module with a 1.58mm focal length fisheye 185 degrees FOV lens and mount it facing forwards on the aerial carrier, moreover we selected the lightweight and small-size DJI N3 flight controller embedded with an inertial measurement unit (IMU) module which can provide 400Hz inertial measurements and gyroscope data working with 15Hz synchronized fisheye images to run the localization algorithm described in Section 3. We selected the lightweight commercial stereo camera module Intel RealSense D435i which is mounted on the upper front of the protection frame and can output raw point cloud data at 30Hz, RGB images, IMU data, and depth images for environmental mapping. To allow all aerial carrier software running onboard, a powerful mini sized PC Intel NUC7i7DNBE is utilized to process all sensors and actuation data and to communicate with the onboard autopilot and ground station, depicted in Figure 2. To monitor the system status and command the

aerial carrier and companion UAV, a ground station was equipped with a ThinkPad PC communicating with the aerial systems via WiFi and a RC controller to command the system operation via radio signal.

2.4 Power Management

As shown in Figure 2, two 4S LiPo batteries provide stable power supply for the onboard aerial carrier using two UBEC modules and the power budget of all the components are listed in Table 2 which meets the requirement of the maximum operation time of eight minutes.

Table 2: System power budget.

Component	Input voltage(V)	MP(W)
DC motor ESC	14.80	493.00×4
Onboard PC	12.00	59.31
Dynamixel servo	5.00	7.35 × 2
Autopilot	14.80	4.80
Fisheye camera	3.30	0.40
D435i stereo	5.00	2.50

MP: Maximum power.

3 SOFTWARE AND ALGORITHM DESIGN

In this section, we address the software components for the aerial carrier platform to achieve transportation and automatic anchoring operation.

3.1 Software Overview

Figure 4 provides an overview of system software modules and architecture implemented on the aerial carrier for stable position flight control, map formation, and the control of the anchoring mechanism.

The positioning module's functionality is to provide the pose information for the mapping algorithm and feedback for the position controller. Due to this positioning module and by using its D435i stereo camera, the aerial carrier is capable of generating 3D maps of its environment that can be used by a human operator for further analysis. For stable flight control e.g., during transportation, a position controller for the aerial carrier has been developed considering the platform dynamics. For reliable anchoring of the companion UAV, a software has been designed and implemented that allows automatic anchoring. As shown in Figure 4, all software modules are managed by a finite state machine (FSM) to accomplish the transport and anchoring tasks effectively.

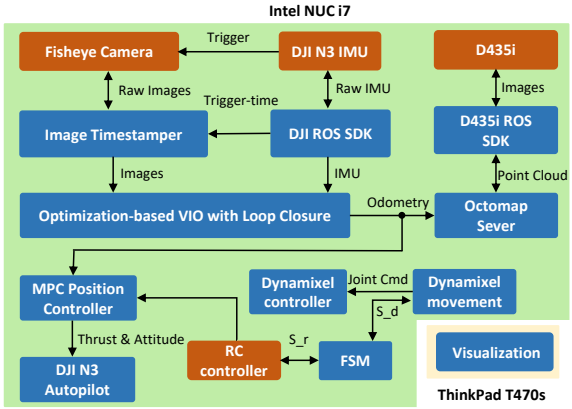

Figure 4: System software architecture.

3.2 Positioning and Mapping

Precise positioning, being pose feedback information in position control loop, is a key factor to keep the aerial carrier stable during transportation and anchoring. Due to the consideration of the platform configuration and our experiment environment, IMU data and vision data are tightly fused into a visual inertial odometry pipeline to output a reliable and accurate pose (Qin et al., 2018; Qin and Shen, 2018). To implement this pipeline on this aerial platform, hardware synchronization of the IMU and monocular vision data is essential for this application and required by its high accuracy of the positioning. As shown in Figure 4, hardware synchronization is implemented by the DJI N3 autopilot IMU that is triggering the camera image capture at a fixed frequency of 15Hz. The image data is stamped with the corresponding IMU timestamp for further processing. Strictly, the sampling data is not in complete temporal alignment because of the image exposure and data transmission delay (Qin and Shen, 2018). However, the time offset between IMU and images can be estimated online along with this optimization based positioning system (Qin et al., 2018). This positioning system with its loop closure outputs data at 15Hz including the position, orientation, linear and angular velocity of the aerial platform body with respect to the inertia frame whose origin is aligned with the positioning system's initialization point. To increase the frequency of the localization system, the positioning system output is directly propagated with IMU data as in (Qin et al., 2018; Lin et al., 2018) and the final system provides the localization information at 80Hz which is sufficient to be feed back to the position controller. Using the precise localization information and the point cloud data from the stereo camera, we employ a mapping algorithm Octomap server (Hornung et al., 2013) to obtain a volumetric 3D occupancy map which is

applicable to environment perception and path generation.

3.3 Motion Control

In the aerial robot control field, cascaded connection of a high level controller and a low level controller is a typical approach to control the aerial robot flying at a desired pose. We employ an off-the-shelf autopilot DJI N3 as the low level attitude controller, which enables the dynamics of the aerial platform to be approximated. In cooperation with the tuned low level controller, a position nonlinear MPC controller with the pose command from RC controller, closely related to some previous work (Kamel et al., 2017; Kamel et al., 2016; Tzoumanikas et al., 2019; Carlos et al., 2020), is developed and implemented onboard to generate the pitch, roll, and thrust command for the autopilot while considering external environmental disturbances. Moreover, in the algorithm the the dynamics of the aerial platform are approximated with RC data and IMU data, and the pitch and roll constraints are both set to 20 degrees and thrust command constraints is set to 120N. An EKF-based disturbance estimator is used within the nonlinear MPC controller. Subject to the yaw control, a typical P controller is utilized to generate a yaw rate command.

3.4 Anchor Operation

Two servo motors Dynamixel XL330-M288 operate in position mode and are controlled by the ROS Dynamixel workbench which can provide high precision joint position tracking. In order to operate the arms of the anchoring mechanism automatically, the ROS execution service is called to either drive them smoothly to their opening or closing position with the motor speed 1.57rad/s depending on the desired state of the system with the RC controller triggering.

3.5 Finite State Machine

The behavior of the aerial platform is determined by a finite state machine (FSM) consisting of three states:

- *RC control*: This is the initial state for the aerial platform taking off, normal landing or emergency landing. After the take-off is completed and it is hovering stably, the FSM transitions to the *Transportation* state.
- *Transportation*: The aerial platform is moving with the command from RC controller. When it reaches the hover position and hovers stably, the state switches to *Anchor operation*. In case of emergency, the state switches to *RC control* to conduct emergence landing.
- *Anchor operation*: In this state, the anchor is starting to work for locking or releasing the companion UAV with a RC switch triggering. When the action is done, the FSM transitions to the *Transportation* state or it transitions to *RC control* if an emergency is triggered.

4 EXPERIMENTAL RESULTS

In this section, we conduct multiple experiments to evaluate the performance of the aerial carrier platform and the anchor operation for the companion UAV.

4.1 Aerial Transportation

Before implementing the nonlinear MPC controller, the first-order and second-order inner loop attitude control dynamical model of the aerial platform is identified as described in (Sa et al., 2018) to obtain the approximation of the attitude control loop dynamic. The model identification results are presented in Table. 3, and

Table 3: Identification of attitude control loop dynamical model.

Model	ϕ	θ
First-order model	$k_\phi = 1.738$	$k_\theta = 1.303$
	$\tau_\phi = 0.182$	$\tau_\theta = 0.154$
Second-order model	$k_\phi = 1.572$	$k_\theta = 1.168$
	$\omega_\phi = 6.061$	$\omega_\theta = 5.494$
	$\zeta_\phi = 0.356$	$\zeta_\theta = 0.327$

$k_{\{.\}}$ are the model gains, $\tau_{\{.\}}$ are the time constants, $\omega_{\{.\}}$ are the damping constants, and $\zeta_{\{.\}}$ are the natural frequencies.

In practice, to conduct aerial transportation, the flight control of the aerial platform is a critical factor. To evaluate the stability and effectiveness of the MPC controller with the onboard positioning module outputs at 80Hz, the drone is hovering at one waypoint and the hovering result is depicted in Figure 5, and average error of the x and z axis are both less than 0.05m and the average error of the y axis is less than 0.09m. The MPC controller output results are shown in Figure 6 and the commands for the attitude controller input are within the range of the attitude and thrust constraints, and the thrust command is scaled based on the DJI autopilot input requirement. Additionally, the aerial carrier is equipped with the ability to conduct environment mapping which can be used

for transportation flight path planning. As shown in Figure 7, the real-time updated 3D occupancy 10cm-resolution mapping is generated with the OctoMap framework in a lab environment depicted in Figure 8.

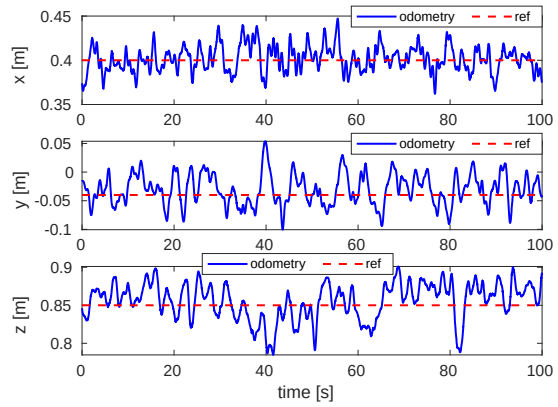

Figure 5: Hover flight test with odometry.

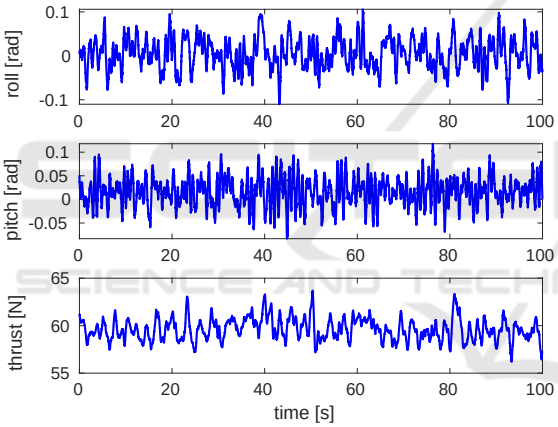

Figure 6: Roll, pitch, and thrust command for the aerial carrier.

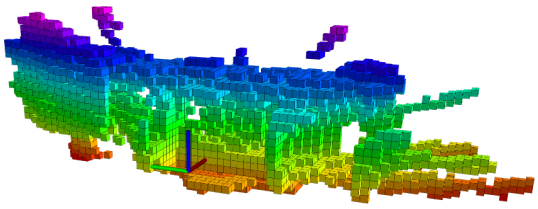

Figure 7: 3D occupancy map with OctoMap framework.

4.2 Anchor Test

To test the the effectiveness and reliability of the anchor system, firstly we configure different numbers of companion UAV feet grabbed as shown in Figure 9. Subject to each configuration of the number of the feet grabbed, we do 30 sampling tests with the carrier wobbling with pitch and roll angles of 90 degrees respectively, and the results of locking success rate with different numbers of feet grabbed are presented in Figure 10 which indicates that with more than 2 feet grabbed the locking performance is reliable and sufficient for our application.

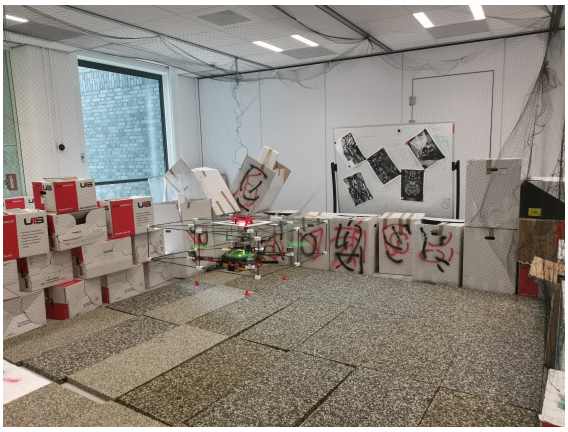

Figure 8: Lab environment used for flight experiments.

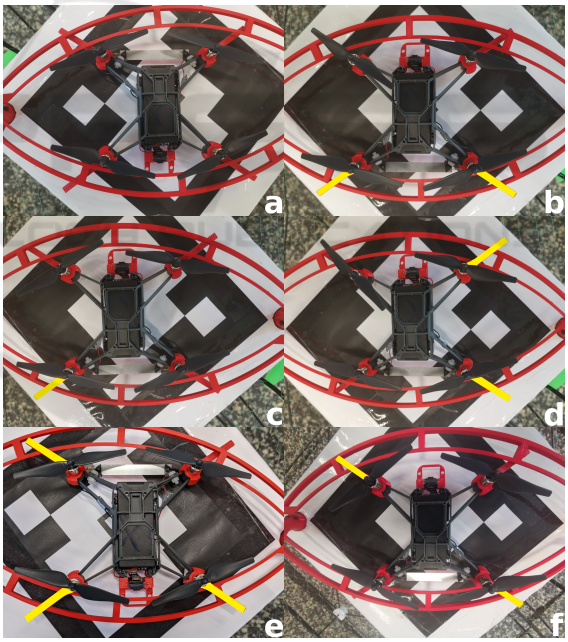

Figure 9: Grabbed feet configurations. The feet that are not held by the arms are highlighted in yellow. **a)** shows all feet are successfully grabbed by the arms. **c)** shows only one foot being grabbed. **e)** shows three feet being grabbed. **b)**, **d)**, and **f)** present varying two feet configurations.

With reference to the previous UAV landing research in Table 4, the landing error can be less than 8cm and the corresponding requirement of the docking platform profile and size of the companion UAV is included in our design of the docking platform and

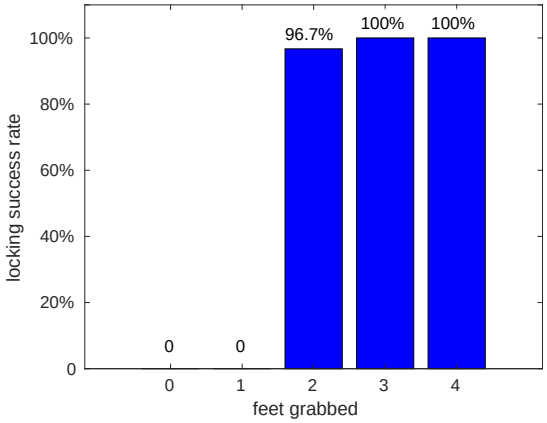

Figure 10: Locking success rate with different number of the feet grabbed.

the choice of the companion UAV.

Table 4: Landing errors of various state-of-the-art UAV landing methods.

Methods	Landing error (cm)
(Yang et al., 2014)	1.5
(Cocchioni et al., 2014)	2.0
(Benini et al., 2016)	2.0
(Yu et al., 2017)	0.4
(Alvarez Custodio, 2019)	7.8
(Sani and Karimian, 2017)	6.0

To obtain the proper docking orientation in yaw and find the better docking success rate, the docking anchoring experiments on the ground are conducted when the companion UAV with four anchor feet docks on the docking fractal marker board with a yaw angle of 0 degrees, 30 degrees, and 45 degrees, respectively, and the coordinate system of the companion UAV and docking platform are described in Figure 11. As shown in Figure 12 for experiments with a docking yaw angle of 0 degrees, the maximum docking center offset can reach $\pm$8cm with the rotational symmetry test data mirroring, but only 52.7% of the samples are grabbed by three or four feet, and based on the results in Figure 10 and Table 4, it suggests that the companion UAV can reliably dock with the yaw angle of 0 degrees and offset $\pm$8cm. The experiment results of docking with a yaw angle of 30 degrees are shown in Figure 13, and the samples grabbed with three or four feet occupy around 96.67% but the maximum docking center offset is only around $\pm$6.5cm. Moreover, the results of docking with a yaw angle of 45 degrees are presented in Figure 14 and all the sampling cases are grabbed with three or four feet, but the the maximum docking center offset is only around $\pm$6.7cm. Based on the results of the three cases above, it indicates that docking with a yaw angle of 45 degrees is relatively reliable and robust, but its docking available area is small, which requires higher landing accuracy for the companion UAV. Specially noted, if the companion UAV is grabbed with more than two feet during flight tests, it will be automatically centered by the drone's high-frequency shaking and the force applied by the two servo motors.

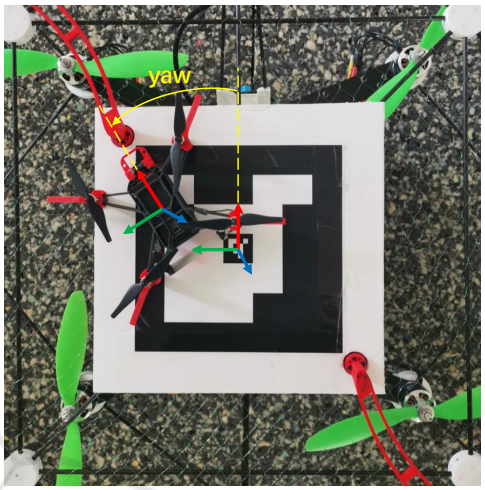

Figure 11: Coordinate system.

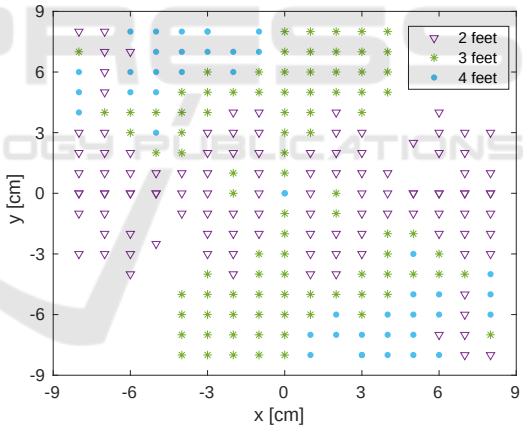

Figure 12: Companion UAV grab test with yaw angle of 0 degrees.

In mechanic design, we adapt a net protection structure to ensure the safety of the carrier when the docking fails on the tag board. We intentionally place the drone with yaw angle of 0 degrees on sampling points of the nets protection structure while the drone is wobbling with pitch and roll angles of 45 degrees respectively to test its ability to hold the companion UAV in place in order to demonstrate its fault-tolerance. The result is displayed in Figure 15.

It suggests that the companion UAV docking with error of around $\pm 0.35m$ can be safe and will not destroy the carrier, docking platform or itself.

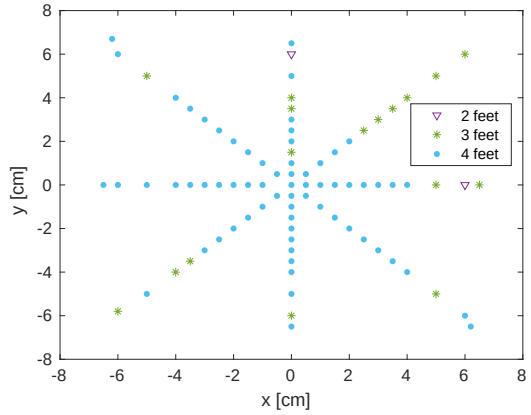

Figure 13: Companion UAV grab test with yaw angle of 30 degrees.

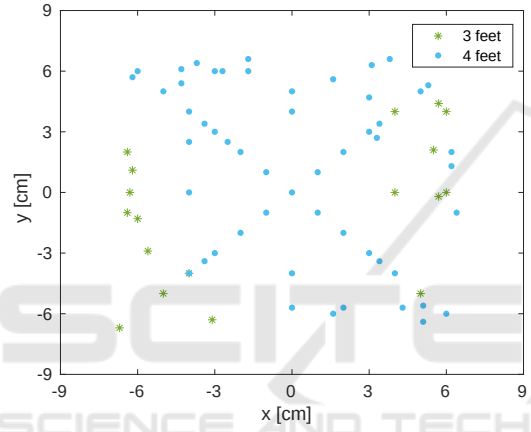

Figure 14: Companion UAV grab test with yaw angle of 45 degrees.

5 CONCLUSIONS

In this paper, we present the system design of an aerial carrier and anchoring platform for transporting a companion UAV. To fulfill the aerial carrier flight implementation, an aerial system including precise localization, environment perception, and flight control framework was developed and implemented in an indoor lab environment. Subject to the anchoring platform, we designed a customized lightweight anchor system to lock the companion UAV and a fault-tolerant protection structure to ensure the docking security. The effectiveness and reliability of them are validated by the experiments with different configurations of feet grabbed and docking orientations. The future work will focus on the outdoor real-world in-flight companion UAV docking experiments with our aerial carrier and anchoring platform.

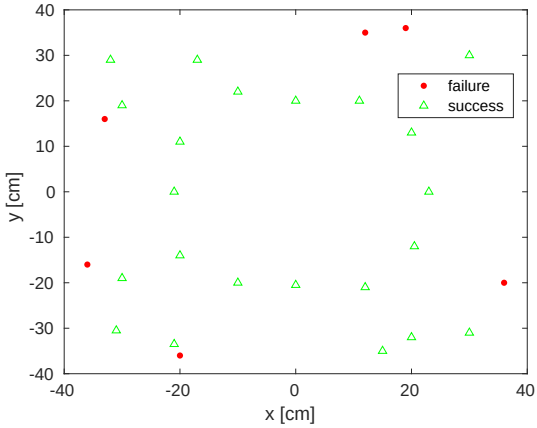

Figure 15: Nets docking fault-tolerance test.

ACKNOWLEDGEMENTS

This research received financial support by a Luik-3 grant on advanced brain-robot interfaces.

REFERENCES

Afrisal, H., Rahmadani, T., Nugroho, W. D., Putra, D. A., et al. (2019). Inertial navigation system of quadrotor based on imu and gps sensors. In *2019 6th International Conference on Information Technology, Computer and Electrical Engineering (ICITACEE)*, pages 1–6. IEEE.

Alvarez Custodio, M. (2019). Autonomous recharging system for drones: Detection and landing on the charging platform.

Benini, A., Rutherford, M. J., and Valavanis, K. P. (2016). Real-time, gpu-based pose estimation of a uav for autonomous takeoff and landing. In *2016 IEEE International Conference on Robotics and Automation (ICRA)*, pages 3463–3470. IEEE.

Bloesch, M., Burri, M., Omari, S., Hutter, M., and Siegwart, R. (2017). Iterated extended kalman filter based visual-inertial odometry using direct photometric feedback. *The International Journal of Robotics Research*, 36(10):1053–1072.

Carlos, B. B., Sartor, T., Zanelli, A., Frison, G., Burgard, W., Diehl, M., and Oriolo, G. (2020). An efficient real-time nmpc for quadrotor position control under communication time-delay. In *2020 16th International Conference on Control, Automation, Robotics and Vision (ICARCV)*, pages 982–989. IEEE.

Cocchioni, F., Mancini, A., and Longhi, S. (2014). Autonomous navigation, landing and recharge of a quadrotor using artificial vision. In *2014 international conference on unmanned aircraft systems (ICUAS)*, pages 418–429. IEEE.

Daudelin, J., Jing, G., Tosun, T., Yim, M., Kress-Gazit, H., and Campbell, M. (2018). An integrated system for

perception-driven autonomy with modular robots. *Science Robotics*, 3(23).

Garrido-Jurado, S., Munoz-Salinas, R., Madrid-Cuevas, F. J., and Medina-Carnicer, R. (2016). Generation of fiducial marker dictionaries using mixed integer linear programming. *Pattern Recognition*, 51:481–491.

Hornung, A., Wurm, K. M., Bennewitz, M., Stachniss, C., and Burgard, W. (2013). OctoMap: An efficient probabilistic 3D mapping framework based on octrees. *Autonomous Robots*. Software available at http://octomap.github.com.

Jain, K. P. and Mueller, M. W. (2020). Flying batteries: In-flight battery switching to increase multirotor flight time. In *2020 IEEE International Conference on Robotics and Automation (ICRA)*, pages 3510–3516. IEEE.

Jain, K. P., Park, M., and Mueller, M. W. (2020). Docking two multirotors in midair using relative vision measurements. *arXiv preprint arXiv:2011.05565*.

Kamel, M., Burri, M., and Siegwart, R. (2016). Linear vs Nonlinear MPC for Trajectory Tracking Applied to Rotary Wing Micro Aerial Vehicles. *ArXiv e-prints*.

Kamel, M., Stastny, T., Alexis, K., and Siegwart, R. (2017). Model predictive control for trajectory tracking of unmanned aerial vehicles using robot operating system. In Koubaa, A., editor, *Robot Operating System (ROS) The Complete Reference, Volume 2*. Springer.

Lee, T., Leok, M., and McClamroch, N. H. (2010). Geometric tracking control of a quadrotor uav on se (3). In *49th IEEE conference on decision and control (CDC)*, pages 5420–5425. IEEE.

Lin, Y., Gao, F., Qin, T., Gao, W., Liu, T., Wu, W., Yang, Z., and Shen, S. (2018). Autonomous aerial navigation using monocular visual-inertial fusion. *Journal of Field Robotics*, 35(1):23–51.

Lin, Y.-C., Cheng, Y.-T., Zhou, T., Ravi, R., Hasheminasab, S. M., Flatt, J. E., Troy, C., and Habib, A. (2019). Evaluation of uav lidar for mapping coastal environments. *Remote Sensing*, 11(24):2893.

Loianno, G., Spurny, V., Thomas, J., Baca, T., Thakur, D., Hert, D., Penicka, R., Krajnik, T., Zhou, A., Cho, A., et al. (2018). Localization, grasping, and transportation of magnetic objects by a team of mavs in challenging desert-like environments. *IEEE Robotics and Automation Letters*, 3(3):1576–1583.

Lutz, P., Müller, M. G., Maier, M., Stoneman, S., Tomić, T., von Bargen, I., Schuster, M. J., Steidle, F., Wedler, A., Stürzl, W., et al. (2020). Ardea—an mav with skills for future planetary missions. *Journal of Field Robotics*, 37(4):515–551.

Narváez, E., Ravankar, A. A., Ravankar, A., Emaru, T., and Kobayashi, Y. (2020). Autonomous vtol-uav docking system for heterogeneous multirobot team. *IEEE Transactions on Instrumentation and Measurement*, 70:1–18.

Narváez, E., Ravankar, A. A., Ravankar, A., Kobayashi, Y., and Emaru, T. (2017). Vision based autonomous docking of vtol uav using a mobile robot manipulator. In *2017 IEEE/SICE International Symposium on System Integration (SII)*, pages 157–163. IEEE.

Peng, K., Du, J., Lu, F., Sun, Q., Dong, Y., Zhou, P., and Hu, M. (2019). A hybrid genetic algorithm on routing and scheduling for vehicle-assisted multi-drone parcel delivery. *IEEE Access*, 7:49191–49200.

Perez-Grau, F. J., Caballero, F., Merino, L., and Viguria, A. (2017). Multi-modal mapping and localization of unmanned aerial robots based on ultra-wideband and rgb-d sensing. In *2017 IEEE/RSJ International Conference on Intelligent Robots and Systems (IROS)*, pages 3495–3502. IEEE.

Qin, T., Li, P., and Shen, S. (2018). Vins-mono: A robust and versatile monocular visual-inertial state estimator. *IEEE Transactions on Robotics*, 34(4):1004–1020.

Qin, T. and Shen, S. (2018). Online temporal calibration for monocular visual-inertial systems. In *2018 IEEE/RSJ International Conference on Intelligent Robots and Systems (IROS)*, pages 3662–3669. IEEE.

Rocha, R. and Robinson, S. K. (2020). Toward autonomous in-flight docking of unmanned multi-rotor aerial vehicles. In *AIAA Scitech 2020 Forum*, page 1486.

Romero-Ramire, F. J., Munoz-Salinas, R., and Medina-Carnicer, R. (2019). Fractal markers: a new approach for long-range marker pose estimation under occlusion. *IEEE Access*, 7:169908–169919.

Romero-Ramirez, F. J., Muñoz-Salinas, R., and Medina-Carnicer, R. (2018). Speeded up detection of squared fiducial markers. *Image and vision Computing*, 76:38–47.

Sa, I., Kamel, M., Khanna, R., Popović, M., Nieto, J., and Siegwart, R. (2018). Dynamic system identification, and control for a cost-effective and open-source multi-rotor mav. In *Field and Service Robotics*, pages 605–620. Springer.

Sani, M. F. and Karimian, G. (2017). Automatic navigation and landing of an indoor ar. drone quadrotor using aruco marker and inertial sensors. In *2017 international conference on computer and drone applications (IConDA)*, pages 102–107. IEEE.

Tzoumanikas, D., Li, W., Grimm, M., Zhang, K., Kovac, M., and Leutenegger, S. (2019). Fully autonomous micro air vehicle flight and landing on a moving target using visual–inertial estimation and model-predictive control. *Journal of Field Robotics*, 36(1):49–77.

Ullah, N., Mehmood, Y., Aslam, J., Ali, A., and Iqbal, J. (2021). Uavs-ugv leader follower formation using adaptive non-singular terminal super twisting sliding mode control. *IEEE Access*, 9:74385–74405.

Wasim, M., Ullah, M., and Iqbal, J. (2019). Gain-scheduled proportional integral derivative control of taxi model of unmanned aerial vehicles. *Revue Roumaine des Sciences Techniques-Serie Electrotechnique et Energetique*, 64(1):75–80.

Yang, S., Scherer, S. A., Schauwecker, K., and Zell, A. (2014). Autonomous landing of mavs on an arbitrarily textured landing site using onboard monocular vision. *Journal of Intelligent & Robotic Systems*, 74(1):27–43.

Yu, C., Cai, J., and Chen, Q. (2017). Multi-resolution visual fiducial and assistant navigation system for unmanned

aerial vehicle landing. *Aerospace Science and Technology*, 67:249–256.

Yu, K., Budhiraja, A. K., and Tokekar, P. (2018). Algorithms for routing of unmanned aerial vehicles with mobile recharging stations. In *2018 IEEE International Conference on Robotics and Automation (ICRA)*, pages 5720–5725. IEEE.

Zhang, J. and Singh, S. (2014). Loam: Lidar odometry and mapping in real-time. In *Robotics: Science and Systems*, volume 2.